# Synthetic Affibody Molecules: A Novel Class of Affinity Ligands for Molecular Imaging of HER2-Expressing Malignant Tumors

Anna Orlova,[1,2] Vladimir Tolmachev,[1,2] Rikard Pehrson,[1] Malin Lindborg,[1] Thuy Tran,[2] Mattias Sandström,[3] Fredrik Y. Nilsson,[1,2] Anders Wennborg,[1] Lars Abrahmsén,[1] and Joachim Feldwisch[1,2]

[1]Affibody AB, Bromma, Sweden; [2]Department of Oncology, Radiology and Clinical Immunology, Rudbeck Laboratory, Uppsala University; and [3]Department of Hospital Physics, Uppsala University Hospital, Uppsala, Sweden

## Abstract

**The Affibody molecule $Z_{HER2:342\text{-}pep2}$, site-specifically and homogeneously conjugated with a 1,4,7,10-tetra-azacylododecane-*N,N′,N″,N‴*-tetraacetic acid (DOTA) chelator, was produced in a single chemical process by peptide synthesis. DOTA-$Z_{HER2:342\text{-}pep2}$ folds spontaneously and binds HER2 with 65 pmol/L affinity. Efficient radiolabeling with >95% incorporation of $^{111}$In was achieved within 30 min at low (room temperature) and high temperatures (up to 90°C). Tumor uptake of $^{111}$In-DOTA-$Z_{HER2:342\text{-}pep2}$ was specific for HER2-positive xenografts. A high tumor uptake of 23% injected activity per gram tissue, a tumor-to-blood ratio of >7.5, and high-contrast gamma camera images were obtained already 1 h after injection. Pretreatment with Herceptin did not interfere with tumor targeting, whereas degradation of HER2 using the heat shock protein 90 inhibitor 17-allylaminogeldanamycin before administration of $^{111}$In-DOTA-$Z_{HER2:342\text{-}pep2}$ obliterated the tumor image. The present results show that radiolabeled synthetic DOTA-$Z_{HER2:342\text{-}pep2}$ has the potential to become a clinically useful radiopharmaceutical for *in vivo* molecular imaging of HER2-expressing carcinomas.** [Cancer Res 2007;67(5):2178–86]

## Introduction

The concept of personalized medicine involves both novel selective targeting therapeutics adapted for treatment of defined disease stages and means to diagnose and stratify the patient population that may respond to these treatments (1). Currently used noninvasive imaging techniques, such as anatomic imaging by computer tomography and metabolic imaging using $^{18}$F-fluorodeoxyglucose ($^{18}$F-FDG), do not provide molecular information on oncological target molecules. In contrast, tumor marker–targeted molecular imaging can biochemically characterize the imaged structures in the body, thereby adding new qualitative information to these images not available today (e.g., for assessing the aggressiveness of cancer and for monitoring of targeted therapy; ref. 2). A targeting agent suitable for molecular imaging should be able to specifically target relevant pathologic structures in the body, while avoiding normal tissue (3, 4). In patients, it should quickly find its target while unbound molecules should be rapidly excreted, thus facilitating high-contrast imaging and reducing the time required for the examination. For clinical development, site-specific, homogeneous, reproducible, and easy radiolabeling is desirable. However, the most commonly used class of targeting agents (i.e., antibodies and various antibody derived fragments) are usually modified at multiple and randomly distributed sites by using modification chemistries based on amine, thiol, or tyrosine-reactive reagents (5). Thus, the resulting targeting molecules are heterogeneous preparations with various degrees of modification (6, 7).

The clinical use of antibodies for molecular imaging is limited due to their long biodistribution times, slow tumor penetration, and slow blood clearance. Improved imaging agents have been obtained by using smaller antibody fragments that have faster biodistribution and more rapid blood and whole body clearance (8). However, even the mass of the smallest fragments (27-54 kDa) may not be small enough to allow for efficient extravasation, good tissue penetration, and fast blood clearance (9). Pretargeting of bispecific antibodies followed by administration of radiolabeled small peptides have shown high tumor signal intensities, improved tumor-to-blood (T/B) ratios, and contrasts (10). However, pretargeting is a multistep process whose practical clinical use may be hampered by the prolonged treatment regimes of the 24 to 48 h required before injection of the radiolabeled peptide. Short peptides, on the other hand, are small and have very rapid kinetics, but there is a limited repertoire of natural peptides to choose from (11, 12), and peptides derived from phage display libraries seldom have the high affinity to be considered a general class of targeting molecules (13).

Affibody molecules are small non-immunoglobulin affinity ligands based on a 58-amino-acid Z-domain scaffold, derived from one of the IgG-binding domains of staphylococcal protein A (14). Randomization of 13 amino acid positions in the binding surface of this domain scaffold has been used for construction of combinatorial phagemid libraries, from which Affibody molecules binding desired target molecules can be selected by phage display (15, 16). Thus, the Affibody molecule with binding specificity for the target human epidermal growth factor receptor 2 (HER2, also known as Neu and ErbB2) described here differs from other Affibody molecules (e.g., a Taq polymerase–specific Affibody molecule; ref. 16), only in the 13 amino acids that form the target binding site.

HER2 is overexpressed in a number of carcinomas and is associated with shorter time to disease progression and decreased overall survival in breast cancer patients (17–19). Noninvasive detection of HER2 expression by novel imaging radiopharmaceuticals could become an important complement to immunohistochemistry or fluorescence *in situ* hybridization, allowing the

**Note:** The phrase "Affibody molecule" is used in this publication instead of "Affibody® molecule." Affibody is a trademark owned by Affibody AB. Affibody is a trademark registered in Sweden, Europe, and the United States and under trademark application in Japan.

**Requests for reprints:** Joachim Feldwisch, Affibody AB, Voltavägen 13, P.O. Box 20137, SE-16102 Bromma, Sweden. Phone: 46-859883852; Fax: 46-859883801; E-mail: joachim.feldwisch@affibody.com.



doi:10.1158/0008-5472.CAN-06-2887

identification of HER2-positive metastases not amenable to biopsy. One potential clinical application is the identification of patients where metastases from HER2-negative primary breast tumors are HER2-positive and thus may respond to trastuzumab treatment (20). Furthermore, imaging of HER2 expression could provide a direct readout of the efficacy of pharmaceuticals aimed to interfere with HER2 overexpression, such as 17-allylamino-geldanamycin (17-AAG), which belongs to a new class of heat shock protein 90 (HSP90) inhibitors (7, 21). HSP90 is a molecular chaperone that is overexpressed in a large number of cancers, including breast cancer. This protein is crucial for folding of a large number of client proteins involved in growth control, cell survival, and development processes, like receptors, kinases, and transcription factors. Thus, inhibition of HSP90 leads to increased proteasome-mediated degradation of client proteins, which in turn leads to inhibition of cell proliferation and finally to apoptosis (22).

Our earlier work has indicated a large potential of Affibody molecules for imaging of HER2-overexpressing tumors. The first generation of HER2-specific Affibody molecules ($His_6$-$Z_{HER2:4}$) bind HER2 with a $K_D$ of 50 nmol/L (23). Dimerization of this Affibody molecule $(Z_{HER2:4})_2$ resulted in improved target binding affinity ($K_D \sim 3$ nmol/L), and radioiodination of recombinantly produced $His_6$-$(Z_{HER2:4})_2$ allowed selective targeting and imaging of HER2-expressing xenografts *in vivo* (24). The second-generation HER2-specific Affibody molecule ($His_6$-$Z_{HER2:342}$) was obtained by affinity maturation (25). $His_6$-$Z_{HER2:342}$ binds HER2 with a $K_D$ of 22 pmol/L, and radioiodination of the monomeric form resulted in good tumor targeting and imaging. Further improvement was obtained using $^{111}$In-labeled benzyl-DTPA-$His_6$-$Z_{HER2:342}$ (26). However, all Affibody molecules described thus far were produced by recombinant expression in *Escherichia coli*, and radiolabeling was done using labeling chemistries relying on amine or thiol-reactive reagents. Thus, similar to antibodies or antibody fragments, these radiolabeled Affibody molecules are heterogeneous preparations with various degrees of modification.

Here, we describe a synthetic Affibody molecule, which overcomes the limitations of other HER2 imaging agents currently under development. DOTA-$Z_{HER2:342\text{-}pep2}$ is made by peptide synthesis in a single chemical process. This Affibody molecule is site-specifically modified at the $NH_2$ terminus with the chelator 1,4,7,10-tetraazacylododecane-*N*,*N*′,*N*″,*N*‴-tetraacetic acid (DOTA), which can be efficiently labeled with the radiometal indium-111 ($^{111}$In). The properties of this well-defined and homogenous radiopharmaceutical were evaluated *in vivo* in mice carrying xenografts derived from human SKOV-3 ovarian cancer cells.

## Materials and Methods

**General.** Reagents were purchased from the following commercial sources: $^{111}$In chloride, Tyco Healthcare (Solna, Sweden); silica gel–impregnated glass fiber sheets for instant TLC (ITLC SG), Pall Life Sciences, Inc. (Ann Arbor, MI); 50 mg/mL Ketalar, Pfizer (New York, NY); 20 mg/mL Rompun, Bayer (Leverkusen, Germany); 5,000 IE/mL heparin, Leo Pharma (Copenhagen, Denmark); Herceptin (trastuzumab), Roche (Basel, Switzerland); and 17-AAG (17-allylamino-17-demethoxygeldanamycin), Invivogen (San Diego, CA). All cell lines were obtained from the American Type Culture Collection (LGC Promochem, Borås, Sweden) or the European Collection of Animal Cell Cultures (Salisbury, United Kingdom). Data on cellular uptake, biodistribution, and gamma camera images were analyzed by unpaired, two-tailed *t* test using GraphPad Prism (version 4.00 for Windows GraphPad Software, San Diego, CA) to determine any significant differences ($P < 0.05$).

**Animal model.** The animal study was approved by the local Ethics Committee for Animal Research. Female outbreed BALB/c *nu*/*nu* mice were used in all experiments. Xenografts of SKOV-3 (ovary ascites adenocarcinoma), MDA-MB-231, MCF7, BT474 (mammary gland adenocarcinomas), and Ramos (B lymphocyte, Burkitt's lymphoma) were implanted in the left hind leg. The selection of cell lines was based on (*a*) the possibility and ease to generate xenografts and (*b*) the HER2 expression levels. BT474 and SKOV-3 were chosen as cell lines with high HER2 expression level (+4 to +5) and MDA-MB-231 and MCF7 as cell lines with low expression level (+1; ref. 27). The Ramos cell line was chosen as a negative control. The xenografts were allowed to develop up to 100 $mm^3$ for biodistribution and 500 $mm^3$ for imaging studies.

**Peptide synthesis.** The 58-amino-acid-long peptides with a DOTA chelator coupled to the $NH_2$ terminus (DOTA-$Z_{HER2:342\text{-}pep2}$ and DOTA-$Z_{taq4:5}$) were made by standard Fmoc peptide synthesis by Innovagen (Lund, Sweden) or Bachem (Bubendorf, Switzerland). DOTA-mono-NHS-tris(*t*-bu)ester (Macrocyclics, Dallas, TX) was used for $NH_2$-terminal modification of the peptide. The DOTA-peptides were obtained as lyophilized white powder.

**Surface plasmon resonance analysis.** Binding of Affibody molecules to HER2 was analyzed using a Biacore 2000 instrument. The recombinant human ErbB2/Fc chimeric protein, consisting of the extracellular domain of ErbB2 (HER2, $Met^1$-$Thr^{652}$) fused to the Fc region of human IgG1 ($Pro^{100}$-$Lys^{330}$) with a COOH-terminal $His_6$-tag (R&D Systems, Minneapolis, MN), was immobilized (1,540 resonance units) onto a surface of a CM5 sensor chip using amine-coupling chemistry. The extracellular domain of HER2 (HER2-ECD; ref. 28) was immobilized (1,090 resonance units) onto a second surface of the chip to allow comparison with previously published results (25). One surface on the chip was activated and deactivated for use as reference cell. Affibody molecules diluted in HBS-EP buffer [10 mmol/L HEPES, 150 mmol/L NaCl, 3 mmol/L EDTA, 0.005% surfactant P-20 (pH 7.4)] were used as analytes. Three analyte concentrations (6, 20, and 60 nmol/L) were injected in duplicates over the chip using a constant flow rate of 50 μL/min. The total injection time was 3.5 min (association) followed by a wash for 10 min (dissociation). The surface was regenerated with one injection of 25 mmol/L HCl. The response measured in the reference cell and the response from a HBS-EP buffer injection were subtracted from the response measured in the cell with immobilized ErbB2/Fc or HER2-ECD, respectively. For analysis of the binding kinetics, a 2-fold dilution series of the analytes ranging from 6 to 0.19 nmol/L (final concentrations) were injected in duplicates over the chip using a constant flow rate of 50 μL/min. The association phase was 5 min followed by a long dissociation phase (60 min) to account for the slow off rate of the Affibody molecules. The dissociation constant $K_D$, the association rate constant $k_a$, and the dissociation rate constant $k_d$ were calculated using the 1:1 Langmuir binding model with mass transfer correction of the BIAevaluation 4.1 software (Biacore AB, Uppsala, Sweden). For the heating experiment, DOTA-$Z_{HER2:342\text{-}pep2}$ was incubated for 5 min at 90°C in a heating block, allowed to cool to room temperature, and then injected over the chip.

**Radiolabeling.** DOTA-$Z_{HER2:342\text{-}pep2}$ [25 μL, 2 mg/mL in 0.2 mol/L ammonium acetate buffer (pH 5.25)] was mixed with a predetermined amount of $^{111}$In chloride. The mixture was incubated for 30 min or 1 h at different temperatures (room temperature, 37°C, 50°C, and 90°C), and the radiochemical purity was evaluated using ITLC eluted with 0.2 mol/L citric acid (pH 2). Radiolabeled Affibody molecules remained at the origin, whereas free indium migrated with the solvent front. For biological experiments, $^{111}$In-DOTA-$Z_{HER2:342\text{-}pep2}$ was diluted with PBS. Labeling with $^{177}$Lu was done as described above at 60°C for 30 min, yielding a peptide denoted $^{177}$Lu-DOTA-$Z_{HER2:342\text{-}pep2}$. Indirect radioiodination of the recombinant Affibody molecule $His_6$-$Z_{HER2:342}$ was done using the linker molecule *N*-succinimidyl-*p*-(trimethylstannyl)benzoate, which is first labeled with $^{125}$I followed by coupling of the resulting *N*-succinimidyl-*p*-iodobenzoate to amine groups of the protein (25, 29).

***In vitro* cell binding assay.** Cultured SKOV-3 cells were incubated for 1 h at 37°C with $^{111}$In-DOTA-$Z_{HER2:342\text{-}pep2}$ using a 1:1 molar ratio of $^{111}$In-DOTA-$Z_{HER2:342\text{-}pep2}$ to HER2 receptor ($1.2 \times 10^6$ receptors per cell; ref. 30). For blocking experiments, a 100-fold excess of unlabeled Affibody

molecule was added 5 min before the addition of $^{111}$In-DOTA-$Z_{HER2:342-pep2}$. All assays were done in triplicates. After incubation, the medium was collected, and the cells were washed six times with cold serum-free medium followed by treatment with 0.5 mL trypsin-EDTA solution (0.25% trypsin, 0.02% EDTA in buffer; Flow, Irvine, United Kingdom) for 10 min at 37°C. When cells were detached, 0.5 mL complete medium was added to each dish, and the cells were resuspended. The radioactivity associated with the cells and culture media was measured in a gamma counter.

To study cellular retention of radioactivity after interrupted incubation, cultured SKOV-3 cells were incubated for 2 h with $^{111}$In-DOTA-$Z_{HER2:342-pep2}$ or $^{125}$I-labeled $His_6$-$Z_{HER2:342}$ as described above. The dishes were then washed six times with cold serum-free culture medium; fresh complete medium was added; and the cells were incubated at 37°C. At predetermined time points, incubation medium was collected from three culture dishes, and cells were detached from culture dishes by trypsin treatment, as described above. The radioactivity associated with the cells, and the culture medium was measured. The fraction of the cell-associated radioactivity was analyzed as a function of time.

**Biodistribution in tumor-bearing mice.** The mice with xenografts were randomized into groups of four. Animals of the blocking group were s.c. injected with 375 to 500 μg of unlabeled $His_6$-$Z_{HER2:342}$ 1 h before injection of the radiolabeled Affibody molecule. All mice were injected s.c. with 100 μL (1 μg, 100 kBq) of $^{111}$In-DOTA-$Z_{HER2:342-pep2}$. After injection of a lethal dose of Ketalar-Rompun solution, mice were sacrificed by exsanguinations via heart puncture at 1, 4, 12, 24, and 72 h after injection. Animals from the blocking group were sacrificed 4 h after injection. The organs were dissected and weighted, and their radioactivity content was measured in a gamma counter. Radioactivity uptake was calculated as percentage of injected activity per gram tissue (%IA/g).

Pretreatment of SKOV-3 xenografts with Herceptin was done by s.c. injection of 1 mg trastuzumab in PBS 2 days before injection of $^{177}$Lu-DOTA-$Z_{HER2:342-pep2}$. The animals from the Herceptin group were sacrificed 4 h after injection, and %IA/g was compared with animals from the group not treated with Herceptin. Mice with BT474, MDA-MB-231, Ramos, or MCF7 xenografts were s.c. injected with 100 μL (1 μg, 100 kBq) $^{111}$In-DOTA-$Z_{HER2:342-pep2}$. For every tumor model, one group was s.c. injected with 375 μg of unlabeled $His_6$-$Z_{HER2:342}$ 1 h before injection of the radiolabeled Affibody molecule. The mice were sacrificed 4 h after injection.

**Gamma camera studies.** Animals with SKOV-3 xenografts were injected in the tail vein with 3 MBq (3 μg) of $^{111}$In-DOTA-$Z_{HER2:342-pep2}$. The animals were euthanized with a lethal dose of Ketalar/Rompun 1, 2, or 4 h after injection. Imaging was done using a Millenium GE gamma camera equipped with a MEGP collimator at the Department of Nuclear Medicine of Uppsala University Hospital. The specificity of HER2-dependent imaging was assessed by two different experiments. In the first experiment, HER2 receptors were preblocked by s.c. injection of 0.9 mg of unlabeled $His_6$-$Z_{HER2:342}$ in PBS 45 min before injection of $^{111}$In-DOTA-$Z_{HER2:342-pep2}$. One hour after injection of the radiolabeled Affibody molecule, the animals were sacrificed and imaged as described above. In the second experiment, HER2 was degraded using the HSP90 inhibitor 17-AAG. The treated animals received three injections of 50 mg/kg 17-AAG within 24 h with the last dose 3 h before injection of $^{111}$In-DOTA-$Z_{HER2:342-pep2}$. Four hours after injection, the animals were sacrificed and imaged as described above. The scintigraphic results were evaluated visually and analyzed quantitatively using the Hermes software (Nuclear Diagnostics, Stockholm, Sweden). Quantitative analysis was done by drawing equal regions of interest (ROI) over the tumor and the contralateral thigh. Tumor-to-nontumor ratios were calculated based on average count per pixel in a ROI.

## Results

**Analysis and radiolabeling of DOTA-$Z_{HER2:342-pep2}$.** A series of experiments were done to confirm that the synthetic Affibody molecule DOTA-$Z_{HER2:342-pep2}$ folds into an active conformation with retained HER2 target binding activity, including surface plasmon resonance binding assay using Biacore, establishment of methods for labeling with $^{111}$In, and assays to assess the binding activity of $^{111}$In-labeled DOTA-$Z_{HER2:342-pep2}$ to HER2-overexpressing SKOV-3 cells. The recombinantly produced proteins $His_6$-$Z_{HER2:342}$ and $^{125}$I-labeled $His_6$-$Z_{HER2:342}$ with known HER2-binding activity served as positive controls.

The Biacore experiments showed that synthetic HER2-specific Affibody molecules bind with high affinity to their target HER2. The extracellular domain of HER2 (HER2-ECD) or chimeric HER2/Fc fusion protein was immobilized onto a Biacore sensor chip, and binding of the synthetic peptide DOTA-$Z_{HER2:342-pep2}$ was compared with the binding of the recombinantly produced protein $His_6$-$Z_{HER2:342}$ (Fig. 1*A*). The overlay plot shows that similar sensorgrams were obtained for the synthetic Affibody molecule and the recombinant Affibody molecule. Because incorporation of metal ions into DOTA may require harsh conditions like elevated temperatures, DOTA-$Z_{HER2:342-pep2}$ was incubated for 5 min at 90°C, and the binding activity for HER2 was analyzed on the same Biacore chip. As seen on the overlay plot, binding of the DOTA-peptide to HER2 was retained after heating.

The kinetic binding constants of the synthetic and recombinant variants were determined in experiments involving a long dissociation phase to account for the slow off-rate of Affibody molecules. Six different concentrations of the Affibody molecules were injected over Biacore chip surfaces with immobilized HER2-ECD and chimeric HER2/Fc fusion protein, respectively. The

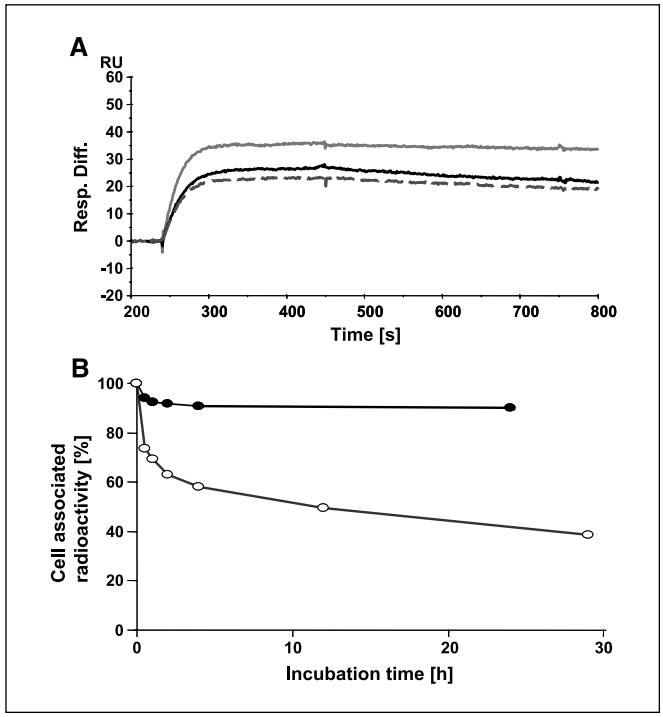


**Figure 1.** Analysis of HER2-binding activity of DOTA-$Z_{HER2:342-pep2}$. *A,* surface plasmon resonance analysis of the interaction of synthetic DOTA-$Z_{HER2:342-pep2}$ (*black line*), synthetic DOTA-$Z_{HER2:342-pep2}$ heated for 5 min at 90°C (*dashed line*), and recombinant $His_6$-$Z_{HER2:342}$ (*gray line*) with chimeric HER2/Fc protein. The sensorgrams were obtained after sequential injection of Affibody molecules (20 nmol/L) over the sensor chip surface containing amine-coupled HER2/Fc chimeric protein. Responses from a buffer injection and a blank sensor chip surface were subtracted. *B,* cell-associated radioactivity as a function of time after interrupted incubation of SKOV-3 cells with $^{111}$In-DOTA-$Z_{HER2:342-pep2}$ (●) and $^{125}$I-labeled $His_6$-$Z_{HER2:342}$ (○). The cell-associated radioactivity at time 0 after the interrupted incubation was considered as 100%. *Points,* mean ($n$ = 3); *bars,* SD. The error bars are smaller than the symbols.

binding affinity of the DOTA-$Z_{HER2:342-pep2}$ was about thrice lower than the recombinant Affibody molecule $His_6$-$Z_{HER2:342}$. The dissociation constants ($K_D = k_d/k_a$) of DOTA-$Z_{HER2:342-pep2}$ were calculated to 65 versus 78 pmol/L for HER2-ECD or chimeric HER2/Fc fusion protein, respectively, and 20 versus 29 pmol/L for $His_6$-$Z_{HER2:342}$. For HER2-ECD, the association rate constants ($k_a$) were determined as $4.0 \times 10^6$ $M^{-1}$ $s^{-1}$ for DOTA-$Z_{HER2:342-pep2}$ and $4.0 \times 10^6$ $M^{-1}$ $s^{-1}$ for $His_6$-$Z_{HER2:342}$, and the dissociation rate constants ($k_d$) were $2.6 \times 10^{-4}$ $s^{-1}$ for DOTA-$Z_{HER2:342-pep2}$ and $8.1 \times 10^{-5}$ $s^{-1}$ for $His_6$-$Z_{HER2:342}$.

DOTA-$Z_{HER2:342-pep2}$ was efficiently labeled with $^{111}$In at slightly acidic conditions. The pH of the final reaction mixture was ~5. The labeling efficiency was evaluated using ITLC, where radiolabeled Affibody molecules remained at the start line of the ITLC sheet, whereas free indium migrated with the solvent front. Under all conditions tested, the labeling efficiency was above 95% of $^{111}$In incorporation, with 96% and 98% after incubation for 30 or 60 min at room temperature, respectively; 98% for both times at 37°C; 99% for both times at 50°C; and 99% for 30 min at 90°C.

Binding specificity tests showed that binding of $^{111}$In-DOTA-$Z_{HER2:342-pep2}$ to living HER2-expressing SKOV-3 cells was receptor mediated because saturation of receptors by preincubation with non-labeled $His_6$-$Z_{HER2:342}$ significantly decreased binding of the radiolabeled Affibody molecule ($P < 0.0001$). The binding specificity was preserved in the whole range of labeling temperatures, from room temperature to 90°C (data not shown). The antigen binding capacity (i.e., percentage of specifically cell-bound radioactivity) was 82 ± 1% after labeling at room temperature and 85.7 ± 0.5% after labeling at 90°C. Cellular retention of $^{111}$In after interrupted incubation of $^{111}$In-labeled DOTA-$Z_{HER2:342-pep2}$ with SKOV-3 cells was measured over time and compared with the retention of $^{125}$I-labeled $His_6$-$Z_{HER2:342}$ (Fig. 1*B*). After an initial reduction, the cell-bound radioactivity remained constant at about 90% of the initially bound activity if the cells were incubated with $^{111}$In-labeled DOTA-$Z_{HER2:342-pep2}$. In contrast, cells incubated with $^{125}$I-labeled $His_6$-$Z_{HER2:342}$ lost about 40% of the original cell associated radioactivity during the first 4 h and additional 20% until 29 h after the interrupted incubation.

**Biodistribution of $^{111}$In-DOTA-$Z_{HER2:342-pep2}$ in xenograft bearing mice.** The next set of experiments assessed the *in vivo* tumor targeting activity and specificity of $^{111}$In-labeled DOTA-$Z_{HER2:342-pep2}$ by analyzing the binding of this molecule to HER2-positive or HER2-negative tumor xenografts and the whole body biodistribution in SKOV-3 xenograft mice. The Taq polymerase–specific Affibody molecule $^{111}$In-DOTA-$Z_{taq4:5}$ served as negative control. In one experiment, $^{177}$Lu-labeled DOTA-$Z_{HER2:342-pep2}$ was used to show that this peptide can be labeled also with other radionuclides.

Biodistribution studies of $^{111}$In-DOTA-$Z_{HER2:342-pep2}$ were done in BALB/c *nu/nu* mice bearing tumor xenografts. As shown in Fig. 2*A*, the radiolabeled Affibody molecule selectively targeted human tumor xenografts of different origin and with different HER2 expression levels. The radioactivity in excised tumors was measured at 4 h after injection and is presented as %IA/g. The highest tumor uptake was seen in tumor xenografts derived from the human breast cancer cell line BT474 with 39.9% IA/g. In xenografts derived from the human ovarian cancer cell line SKOV-3, tumor uptake was 13.3% IA/g, whereas it was 12.4% IA/g in xenografts derived from the human breast cancer cell line MCF7. Even tumor xenografts with low HER2 expression like those derived from the human breast cancer cells MDA-MB-231 showed

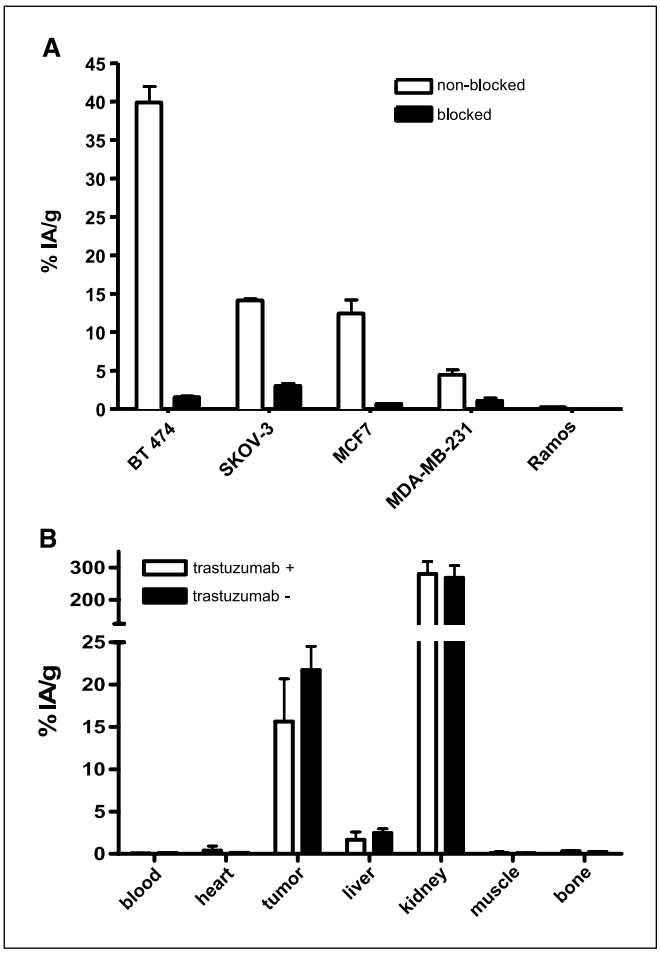


**Figure 2.** Biodistribution of radiolabeled DOTA-$Z_{HER2:342-pep2}$ in BALB/c *nu/nu* mice bearing different tumor xenografts. All animals were s.c. injected with 100 kBq (1 μg) of radiolabeled DOTA-$Z_{HER2:342-pep2}$. *Columns,* mean of four animals per group; *bars,* SD. *A,* tumor targeting of $^{111}$In-DOTA-$Z_{HER2:342-pep2}$ in different xenografts 4 h after injection. Blocking experiments were done using 375 to 500 μg of unlabeled recombinant $His_6$-$Z_{HER2:342}$ in BT474, SKOV-3, MDA-MB-231, and MCF7 xenografts to show specificity of tumor uptake. *B,* biodistribution of $^{177}$Lu-DOTA-$Z_{HER2:342-pep2}$ in SKOV-3 xenografts 4 h after injection, pretreated or not treated with trastuzumab.

specific tumor uptake with 4.4% IA/g. In contrast, no specific tumor uptake was obtained in tumor xenografts derived from the human Ramos B lymphoma cell line with no HER2 expression. *In vivo* targeting of $^{111}$In-DOTA-$Z_{HER2:342-pep2}$ to HER2-expressing tumors could be significantly blocked using excess of unlabeled Affibody molecule $Z_{HER2:342}$ given 1 h before injection of the radiolabeled Affibody molecule ($P < 0.0005$). The reduction of tumor uptake was from 39.9 ± 4.2 to 1.5 ± 0.4% IA/g for BT474 xenografts, 13.3 ± 1.5 to 3.0 ± 0.7% IA/g for SKOV-3 xenografts, and from 12.4 ± 3.1 to 0.7 ± 0.07% IA/g or 4.4 ± 1.4 to 1.1 ± 0.8% IA/g for MCF7 or MDA-MB-231 xenografts, respectively. Because SKOV-3 tumor xenografts can be established with a simpler treatment regime than for BT474 xenografts, further experiments in mice were restricted to SKOV-3 xenografts.

The results of a biodistribution experiment in SKOV-3 xenograft mice are shown in Table 1. The radioactivity in excised organs was measured at 1, 4, 12, 24, and 72 h after injection. The radioactivity concentration in tumor exceeded the radioactivity concentration in all organs and tissues except kidney and at all time points analyzed.

**Table 1.** Biodistribution of $^{111}$In-DOTA-$Z_{HER2:342-pep2}$ and $^{111}$In-DOTA-$Z_{taq4:5}$ in mice bearing SKOV-3 xenografts

| | DOTA-$Z_{HER2:342-pep2}$ | | | | | DOTA-$Z_{taq4:5}$ |
|---|---|---|---|---|---|---|
| | 1 h | 4 h | 12 h | 24 h | 72 h | 4 h |
| Blood | 3.0 ± 0.3 | 1.15 ± 0.05 | 0.80 ± 0.07 | 0.32 ± 0.06 | 0.07 ± 0.01 | 0.13 ± 0.01 |
| Heart | 1.44 ± 0.06 | 0.55 ± 0.07 | 0.49 ± 0.06 | 0.40 ± 0.08 | 0.28 ± 0.06 | 0.09 ± 0.02 |
| Lung | 3.2 ± 0.3 | 0.82 ± 0.07 | 0.86 ± 0.05 | 0.61 ± 0.08 | 0.47 ± 0.07 | 0.17 ± 0.03 |
| Liver | 2.0 ± 0.1 | 1.68 ± 0.05 | 2.2 ± 0.4 | 1.7 ± 0.3 | 1.44 ± 0.06 | 0.46 ± 0.09 |
| Spleen | 1.4 ± 0.2 | 0.61 ± 0.05 | 1.1 ± 0.1 | 1.0 ± 0.3 | 0.91 ± 0.08 | — |
| Pancreas | 0.85 ± 0.08 | 0.27 ± 0.06 | 0.41 ± 0.05 | 0.37 ± 0.04 | 0.29 ± 0.04 | — |
| Kidney | 243 ± 22 | 256 ± 21 | 295 ± 24 | 232 ± 34 | 138 ± 8 | 203 ± 36 |
| Stomach | 1.6 ± 0.2 | 0.41 ± 0.04 | 0.53 ± 0.08 | 0.4 ± 0.2 | 0.33 ± 0.06 | 0.10 ± 0.02 |
| Salivary gland | 1.3 ± 0.1 | 0.7 ± 0.2 | 0.91 ± 0.07 | 0.76 ± 0.05 | 0.71 ± 0.03 | 0.15 ± 0.03 |
| Thyroid* | 0.03 ± 0.02 | 0.02 ± 0.01 | 0.02 ± 0.01 | 0.03 ± 0.01 | 0.01 ± 0.00 | — |
| Tumor | 23 ± 4 | 13 ± 1 (3 ± 0.7)† | 19 ± 2 | 15 ± 2 | 8 ± 2 | 0.13 ± 0.01 |
| Skin | 2.2 ± 0.3 | 0.76 ± 0.09 | 1.3 ± 0.2 | 0.97 ± 0.08 | 0.9 ± 0.1 | 0.37 ± 0.09 |
| Muscle | 0.7 ± 0.1 | 0.3 ± 0.3 | 0.27 ± 0.04 | 0.25 ± 0.08 | 0.17 ± 0.02 | 0.05 ± 0.01 |
| Bone | 1.0 ± 0.2 | 0.7 ± 0.3 | 0.8 ± 0.3 | 0.8 ± 0.4 | 0.7 ± 0.2 | 0.11 ± 0.01 |
| Brain | 0.11 ± 0.04 | 0.04 ± 0.01 | 0.04 ± 0.01 | 0.04 ± 0.01 | 0.03 ± 0.01 | — |

NOTE: Each data point presents an average from four animals ± SD and is expressed as %IA/g of organ or tissue.
*Data for thyroid presented as percentage of injected radioactivity per organ.
†Data in parentheses are given for four animals that were pre-injected with large molar excess of non-labeled Affibody (tumor blocking $P < 0.0001$).

The highest tumor uptake was measured already 1 h after injection with 23% IA/g. The radioactivity measured in the tumor decreased over time, but the rate of this decrease was much slower than the rate of the decrease in the majority of organs. Rapidly decreasing radioactivity concentrations were seen in blood, heart, lung, stomach, and skin. The highest uptake values were measured in the kidneys with a maximum of 295% IA/g at 12 h after injection. Apart from the kidneys, no radioactivity accumulation was detected in excised organs at 4 h after injection, when an Affibody molecule not targeting HER2 (i.e., the Taq polymerase–specific Affibody molecule $^{111}$In-DOTA-$Z_{taq4:5}$) was injected as control (Table 1). The fast blood and organ clearance of $^{111}$In-DOTA-$Z_{HER2:342-pep2}$, in combination with high and sustained tumor uptake, resulted in high T/B and tumor-to-organ (T/O) ratios (Table 2). The T/B ratio was 8 ± 1 at 1 h after injection and increased to 121 ± 33 at 72 h after injection. To investigate if trastuzumab interferes with the tumor targeting of DOTA-$Z_{HER2:342-pep2}$, mice bearing SKOV-3 xenografts were pretreated with trastuzumab 2 days before injection of $^{177}$Lu-DOTA-$Z_{HER2:342-pep2}$. As shown in Fig. 2*B*, uptake of $^{177}$Lu-DOTA-$Z_{HER2:342-pep2}$ was not significantly altered by trastuzumab pretreatment in all organs and tissues investigated. The tumor uptake of $^{177}$Lu-DOTA-$Z_{HER2:342-pep2}$ was 15.6 ± 5.1% IA/g in the trastuzumab-treated group and 21.7 ± 5.6% IA/g in the untreated group. An unpaired *t* test did not reveal any statistically significant difference in tissue uptake between the groups, including tumors ($P = 0.16$).

**Table 2.** T/O ratios for $^{111}$In-DOTA-$Z_{HER2:342-pep2}$ in mice bearing SKOV-3 xenografts

| | 1 h | 4 h | 12 h | 24 h | 72 h |
|---|---|---|---|---|---|
| Blood | 8 ± 1 | 12 ± 2 | 23 ± 4 | 47 ± 14 | 121 ± 33 |
| Heart | 16 ± 4 | 25 ± 4 | 38 ± 5 | 38 ± 12 | 31 ± 11 |
| Lung | 7 ± 2 | 16 ± 2 | 22 ± 4 | 24 ± 4 | 17 ± 4 |
| Liver | 11 ± 2 | 8 ± 1 | 9 ± 2 | 9 ± 2 | 6 ± 1 |
| Spleen | 17 ± 3 | 22 ± 4 | 18 ± 1 | 16 ± 3 | 9 ± 2 |
| Pancreas | 28 ± 8 | 52 ± 19 | 46 ± 8 | 40 ± 9 | 29 ± 8 |
| Kidney | 0.09 ± 0.01 | 0.05 ± 0.01 | 0.06 ± 0.01 | 0.07 ± 0.02 | 0.06 ± 0.02 |
| Stomach | 15 ± 1 | 32 ± 6 | 35 ± 4 | 71 ± 73 | 25 ± 4 |
| Salivary gland | 18 ± 3 | 20 ± 7 | 21 ± 4 | 19 ± 3 | 12 ± 3 |
| Skin | 11 ± 3 | 19 ± 2 | 14 ± 2 | 15 ± 3 | 9 ± 2 |
| Muscle | 36 ± 12 | 53 ± 35 | 68 ± 2 | 65 ± 27 | 48 ± 10 |
| Bone | 24 ± 3 | 17 ± 5 | 29 ± 14 | 23 ± 13 | 13 ± 6 |
| Brain | 240 ± 124 | 392 ± 120 | 431 ± 101 | 393 ± 41 | 369 ± 117 |

NOTE: Each data point presents an average from four animals ± SD.

**Gamma camera imaging.** In the last set of experiments the *in vivo* imaging potential of $^{111}$In-DOTA-$Z_{HER2:342-pep2}$ was investigated. Specificity for HER2 expressing tumors was assessed using competition with unlabeled $His_6$-$Z_{HER2:342-pep2}$ or depletion of HER2 on the tumor cell surface by treatment with 17-AGG.

In clinical practice, early image acquisition is preferred (e.g., 1 h to a few hours after injection). Therefore, a time course experiment was done to investigate the potential of the radiolabeled Affibody molecule for early *in vivo* imaging (Fig. 3*A*). Mice bearing SKOV3 tumor xenografts with an average size of 0.5 $cm^3$ were injected with $^{111}$In-DOTA-$Z_{HER2:342-pep2}$; euthanized at 1, 2, or 4 h after injection; and imaged simultaneously using a gamma camera. High-quality gamma camera images of the tumors with very high contrast to the surrounding tissues were obtained. Besides tumor uptake, substantial kidney retention was seen. Radioactivity accumulation in nontumor tissues slightly exceeded background 1 h after injection but was not seen 1 h later. A blocking experiment was done to prove that the tumor images seen at different time points after injection were due to specific tumor targeting of $^{111}$In-DOTA-$Z_{HER2:342-pep2}$. Two groups of mice were sacrificed 1 h after injection and subjected to simultaneous gamma camera imaging (Fig. 3*B*). In the group pretreated with excess of the unlabeled, recombinant Affibody molecule $His_6$-$Z_{HER2:342}$ tumors could not be visualized, whereas clear tumor targeting was visible in the untreated group. Similar results were obtained if animals were imaged 4 h after injection (data not shown). The specificity of tumor targeting by $^{111}$In-DOTA-$Z_{HER2:342-pep2}$ was further confirmed in an experiment done with an Affibody molecule not targeting HER2. Injection of $^{111}$In-DOTA-$Z_{taq4:5}$ did not target and visualize the SKOV-3 tumor, whereas clear tumor targeting was visible with $^{111}$In-DOTA-$Z_{HER2:342-pep2}$ (Fig. 3*C*).

To further prove the specificity of DOTA-$Z_{HER2:342-pep2}$ for HER2 *in vivo*, animals were treated with the HSP90 inhibitor 17-AAG, a geldanamycin derivative that induces HER2 degradation (Fig. 3*D*). In the group pretreated with 17-AAG 1 day before injection of the radiolabeled Affibody molecule, tumors could not be visualized with $^{111}$In-DOTA-$Z_{HER2:342-pep2}$, or the tumor image intensity was dramatically reduced. In contrast, the tumors were clearly visualized in all untreated animals.

A quantitative ROI analysis over the tumors was done for all images shown in Fig. 3 by drawing equal ROIs over the tumor and the contralateral thigh (Table 3). In animals, which received only $^{111}$In-DOTA-$Z_{HER2:342-pep2}$, the tumor signal was 9 to 27 times higher than the signal measured on the contralateral thigh. However, in animals pretreated with excess of unlabeled Affibody molecule (Fig. 3*B, bottom*) or 17-AAG (Fig. 3*D, bottom*), the tumor signal was significantly reduced to four to eight times over the signal in the contralateral thigh.

## Discussion

In this study, we describe a synthetic Affibody molecule targeting the cell surface receptor HER2, with a single site-specific DOTA chelator modification at the $NH_2$-terminal amino group. Together with facile and efficient radiolabeling, a well-defined and homogeneous radiopharmaceutical is created, which facilitates

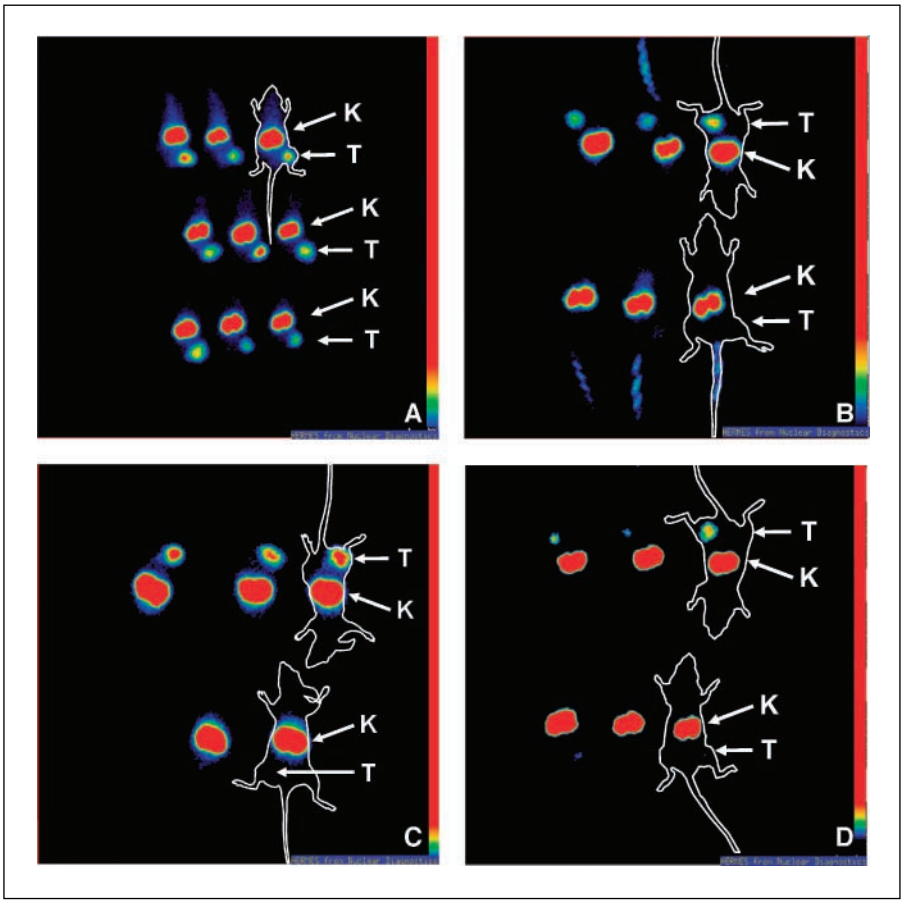


**Figure 3.** Gamma camera images of HER2-expressing SKOV-3 xenograft tumors in BALB/c *nu*/*nu* mice. The time to image acquisition (*A*) and controls to prove imaging specificity for HER2 using competition with unlabeled $Z_{HER2:342}$ (*B*), a negative control Affibody molecule not targeting HER2 (*C*), and drug-induced HER2 degradation (*D*) are shown. All animals were i.v. injected with 3 MBq (3 μg) of $^{111}$In-DOTA-$Z_{HER2:342-pep2}$ or $^{111}$In-DOTA-$Z_{taq4:5}$. Animals were sacrificed by administration of Rompun/Ketalar, and bladders were emptied. Imaging was done using a Millenium GE gamma-camera equipped with a MEGP collimator. To facilitate interpretation, white contours were superimposed around some animals to indicate the location of the animals on the gamma camera screen. Arrows indicate positions of kidneys (*K*) or tumors (*T*). *A,* imaging of mice at different time points after injection, 1 h (*top*), 2 h (*middle*), and 4 h (*bottom*) after injection of $^{111}$In-DOTA-$Z_{HER2:342-pep2}$. *B,* imaging of mice pre-blocked (*bottom*) or not blocked (*top*) with 0.9 mg unlabeled $Z_{HER2:342}$ 45 min before injection of $^{111}$In-DOTA-$Z_{HER2:342-pep2}$. Imaging was done 1 h after injection. *C,* imaging of mice injected with $^{111}$In-DOTA-$Z_{HER2:342-pep2}$ (*top*) or $^{111}$In-DOTA-$Z_{taq4:5}$ (*bottom*) 4 h after injection. *D,* imaging of mice 4 h after injection, pretreated with 17-AAG (*bottom*) and controls (*top*).

**Table 3.** Gamma camera ROI analysis of specific $^{111}$In-DOTA-$Z_{HER2:342-pep2}$ tumor uptake in SKOV-3 xenografts

| | Tumor | Contralateral thigh | Tumor-to-contralateral thigh ratio |
|---|---|---|---|
| Time course | | | |
| 1 h after injection | 271 ± 49 | 29 ± 2 | 9.4 ± 0.9 |
| 2 h after injection | 294 ± 59 | 12 ± 4 | 25 ± 6 |
| 4 h after injection | 218 ± 45 | 9 ± 3 | 27 ± 17 |
| Specificity: block with unlabeled Affibody molecule | | | |
| Non-blocked | 163 ± 40* | 6.6 ± 0.3 | 25 ± 6† |
| Blocked | 32 ± 9* | 8 ± 2 | 4 ± 2† |
| Specificity: 17-AAG treatment | | | |
| Untreated | 126 ± 25‡ | 5 ± 1 | 25 ± 2§ |
| Treated | 60 ± 9‡ | 8 ± 2 | 8 ± 3§ |

NOTE: Equal ROIs were drawn over the tumor and the contralateral thigh of each animal, and the average counts per pixel from three animals ± SD were calculated.
*Significant difference, $P = 0.00501$.
†Significant difference, $P = 0.012$.
‡Significant difference, $P = 0.013$.
§Significant difference, $P = 0.00152$.

further clinical development. Other HER2-targeting imaging agents under development are heterogeneous preparations, usually modified at different and multiple sites. Published values for the average numbers of chelator molecules per ligand ranged from 0.5 to 1.5 for the HER2-specific CHX-A″-C6.5 diabody (31) to 2.6 for DTPA-Fab fragment of trastuzumab (6), 4.7 for DOTA-trastuzumab, and 6.3 for DOTA-$(Fab)_2$ fragments of trastuzumab (7).

The synthetic Affibody molecule DOTA-$Z_{HER2:342-pep2}$ folds spontaneously following chemical synthesis and binds HER2-ECD with a dissociation constant ($K_D$) of 65 pmol/L. This confirms that this Affibody molecule can be produced by chemical synthesis with retained target binding activity. The difference seen in the $K_D$ values for synthetic DOTA-$Z_{HER2:342-pep2}$ and recombinant $His_6$-$Z_{HER2:342}$, which has 11 additional amino acids at the $NH_2$ terminus and no DOTA chelator, could be based on the proximity of the DOTA chelator to the binding surface of the Affibody molecule or differences in the $NH_2$-terminal amino acid sequence. In addition, both synthetic DOTA-$Z_{HER2:342-pep2}$ and recombinant $His_6$-$Z_{HER2:342}$ bind to HER2/Fc fusion protein, however, with a slightly lower affinity ($K_D$ = 78 and 29 pmol/L, respectively) compared with HER2-ECD. The HER2-binding activity is retained after incubation at 90°C as shown by the Biacore and the cell-binding experiments. The high stability and reversible folding of DOTA-$Z_{HER2:342-pep2}$ allows for labeling under harsh conditions, which might be needed for labeling with radiometals other than $^{111}$In. Both high stability and rapid folding may in fact be intrinsic characteristics of Z domain–derived affinity proteins and allows for (re-) gaining the three-helical fold after chemical synthesis or heat denaturation. The substitution of $Gly^{29}$ to alanine, which is the key difference between the Z domain and domain B from protein A, was recently shown to stabilize helix 2 and to increase the rate of folding 3-fold to 3 μs, which is the shortest folding time reported (14, 32).

One of the most important variables for molecular imaging is contrast (i.e., a high signal-to-background ratio; ref. 8). Among the factors that determine imaging contrast is cellular retention of a radiopharmaceutical. Cellular retention depends on the affinity of the Affibody-receptor binding interaction, the rate of Affibody molecule internalization, intracellular degradation, and release of radiocatabolites. The retention curve for $^{111}$In-DOTA-$Z_{HER2:342-pep2}$ indicates stable binding and internalization into SKOV-3 cells and reflects the high affinity of the molecule for the target HER2. Due to the residualizing properties of the $^{111}$In label, the internalized radioactivity remained high over time. In contrast, $His_6$-$Z_{HER2:342}$ labeled with non-residualizing $^{125}$I showed lower retention. Lower tumor uptake and quicker washout of $^{125}$I-labeled $His_6$-$Z_{HER2:342}$ was also seen in experiments *in vivo*, as previously reported (25).

Several attempts to develop noninvasive medical imaging agents suitable for detection of HER2-expressing tumors *in vivo* have been published using radiolabeled HER2-specific antibodies or single-chain Fv (scFv) and Fab or $(Fab)_2$ fragments thereof (6, 7, 33). Other molecules under investigation include minibodies (scFv-Fc fusion proteins; refs. 34, 35) and diabodies (noncovalent scFv dimers; refs. 31, 36). Although successful tumor targeting was shown with radiolabeled antibodies, their clinical use for molecular imaging is limited due to their long biodistribution times, slow tumor penetration, and slow blood clearance, leading to low T/O ratios and low contrasts (37–40). The biodistribution and imaging results obtained with the synthetic DOTA-$Z_{HER2:342-pep2}$ exceed all published data on *in vivo* molecular imaging of HER2 expression. Accumulation of 23% IA/g in the tumor and a T/B ratio of 7.6 at 1 h after injection are exceptional in comparison with the tumor uptake of 2.7% IA/g and T/B of 0.13 obtained for the $^{111}$In-DOTA-$(Fab)_2$ fragment of trastuzumab (7). T/B and T/O ratios at 24 h after injection have been published for several other HER2-targeting imaging agents, and comparison of these results shows that T/B and T/O ratios are at each time point higher for the synthetic Affibody molecule [e.g., T/B was 47 for $^{111}$In-DOTA-$Z_{HER2:342-pep2}$, 19.6 for $^{111}$In-CHX-A″-C6.5 diabody (31), 10.5 for $^{111}$In-DOTA-$(Fab)_2$ fragment of trastuzumab (7), 3.7 for $^{111}$In-DTPA-Fab fragment of trastuzumab (6), and 1.6 for $^{111}$In-DTPA-trastuzumab (33)]. As predicted by the high T/B and T/O values for $^{111}$In-DOTA-$Z_{HER2:342-pep2}$, high-contrast images were obtained as early as 1 h after injection. In contrast, published images with other HER2-targeting agents show weak tumor images, much higher background, and are obtained after 3 to 24 h after injection (6, 7, 21). The use of DOTA as chelator enabled the successful application of the conjugate for imaging. Nearly quantitative and stable binding of $^{111}$In contributed to the observed low uptake of radioactivity into the liver, spleen, and bone.

The only organ with high (and nonspecific) accumulation of the radioactivity was the kidney. This is typical for proteins with a molecular weight below 60 kDa (41). The residualizing properties of $^{111}$In led to long retention of radioactivity. Apparently, this could be an obstacle for imaging of tumors in kidneys or surrounding tissues. However, kidneys are not the main metastatic sites of breast carcinomas (42), the cancer type where $^{111}$In-DOTA-$Z_{HER2:342-pep2}$ may have its first clinical use. Most breast cancer metastases are located at some distance from the kidneys and should therefore be visible by using single-photon emission computed tomography (SPECT).

The high accumulation in the kidneys will probably not restrict the clinical use of $^{111}$In-DOTA-$Z_{HER2:342-pep2}$ because doses of up to 45 Gy as used in radionuclide therapy with $^{111}$In-labeled octreotide showed no negative effect on the kidneys (43, 44). These doses are much higher than the anticipated accumulated kidney doses after

multiple diagnostic imaging with $^{111}$In-DOTA-$Z_{HER2:342-pep2}$. An ample number of publications describe ways to reduce the renal uptake of radiometal-labeled proteins and peptides. The use of positively charged amino acids (41, 45), colchicine (46), and Gelofusine (47) showed positive effects. Further studies with these molecules will show if they can also be used to reduce renal uptake of $^{111}$In-DOTA-$Z_{HER2:342-pep2}$.

Pretreatment of animals with trastuzumab did not interfere with tumor targeting by $^{111}$In-DOTA-$Z_{HER2:342-pep2}$. This result indicates that this radiopharmaceutical might also be used to determine the HER2 status of metastatic lesions in patients with ongoing Herceptin treatment. Thus, DOTA-$Z_{HER2:342-pep2}$ could be used to follow the effect of HER2-targeted therapy with Herceptin and potentially also of other drugs currently under investigation or development, including new antibodies like Omnitarg (pertuzumab), a HER dimerization inhibitor (48), and small molecules, like the HSP90 inhibitor 17-AAG (22) and the tyrosine kinase inhibitor lapatinib (49). Monitoring the presence of drug target and subsequent effect of drug treatment on tumor HER2 levels would be greatly facilitated by molecular imaging in patients using a noninvasive imaging agent. In the present study, we show that $^{111}$In-DOTA-$Z_{HER2:342-pep2}$ can be used to monitor changes in HER2 expression level in animals treated with 17-AAG. Thus, molecular imaging using $^{111}$In-DOTA-$Z_{HER2:342-pep2}$ has the potential to go beyond localization of metastatic lesions *in vivo* by adding new qualitative information not available today by conventional imaging techniques.

Molecules conjugated with a DOTA chelator can not only be labeled with radiometals suitable for SPECT imaging, such as $^{111}$In, but also with positron emitters like $^{68}$Ga for positron emission tomography (PET) imaging. Indeed, a method for $^{68}$Ga labeling of DOTA-$Z_{HER2:342-pep2}$ was recently established, thus broadening the potential clinical applicability of synthetic DOTA-$Z_{HER2:342-pep2}$ for either SPECT or PET (50). Moreover, the present study shows stable attachment of $^{177}$Lu to DOTA-$Z_{HER2:342-pep2}$, opening for the possibility to use a $^{177}$Lu-labeled Affibody molecule for locoregional treatment of urinary bladder carcinomas, which often overexpress HER2 (19). In conclusion, the results presented here show that synthetic DOTA-$Z_{HER2:342-pep2}$ is one of the best available radiopharmaceuticals for *in vivo* molecular imaging of HER2-expressing carcinomas.

## Acknowledgments

Received 8/3/2006; revised 12/6/2006; accepted 1/8/2007.

**Grant support:** Swedish Cancer Society.

The costs of publication of this article were defrayed in part by the payment of page charges. This article must therefore be hereby marked *advertisement* in accordance with 18 U.S.C. Section 1734 solely to indicate this fact.

We thank Lena Israelson for the cell culture work, Veronika Eriksson and staff of the animal facility of Rudbeck laboratory for technical assistance, and Charles Widström (Department of Hospital Physics, Uppsala University Hospital) for help with the gamma camera.



## References

1. Thrall JH. Personalized medicine. Radiology 2004;231:613–6.
2. Wallace AM, Comstock C, Hoh CK, Vera DR. Breast imaging: a surgeon's prospective. Nucl Med Biol 2005;32:781–92.
3. Behr TM, Gotthardt M, Barth A, Behe M. Imaging tumors with peptide-based radioligands. Q J Nucl Med 2001;45:189–200.
4. Britz-Cunningham SH, Adelstein SJ. Molecular targeting with radionuclides: state of the science. J Nucl Med 2003;44:1945–61.
5. Wilbur DS. Radiohalogenation of proteins: an overview of radionuclides, labeling methods and reagents for conjugate labeling. Bioconjug Chem 1992;3:433–70.
6. Tang Y, Wang J, Scollard DA, et al. Imaging of HER2/*neu*-positive BT-474 human breast cancer xenografts in athymic mice using $^{111}$In-trastuzumab (Herceptin) Fab fragments. Nucl Med Biol 2005;32:51–8.
7. Smith-Jones PM, Solit DB, Akhurst T, Afroze F, Rosen N, Larson SM. Imaging the pharmacodynamics of HER2 degradation in response to Hsp90 inhibitors. Nat Biotechnol 2004;22:701–6.
8. Wu AM, Senter PD. Arming antibodies: prospects and challenges for immunoconjugates. Nat Biotechnol 2005;23:1137–46.
9. Michel CC, Curry FE. Microvascular permeability. Physiol Rev 1999;79:703–61.
10. Sharkey RM, Cardillo TM, Rossi EA, et al. Signal amplification in molecular imaging by pretargeting a multivalent, bispecific antibody. Nat Med 2005;11:1250–5.
11. Heppler A, Froidevaux S, Eberle AN, Maecke H. Receptor targeting for tumor localization and therapy with radiopeptides. Curr Med Chem 2000;7:791–4.
12. Reubi JC. Somatostatin and other peptide receptors as tools for tumor diagnosis and treatment. Neuroendocrinology 2004;80:51–6.
13. Landon LA, Deutscher SL. Combinatorial discovery of tumor targeting peptides using phage display. J Cell Biochem 2003;90:509–17.
14. Nilsson B, Moks T, Jansson B, et al. A synthetic IgG-binding domain based on staphylococcal protein A. Protein Eng 1987;1:107–13.
15. Nord K, Nilsson J, Nilsson B, Uhlen M, Nygren PA. A combinatorial library of an alpha-helical bacterial receptor domain. Protein Eng 1995;8:601–8.
16. Nord K, Gunneriusson E, Ringdahl J, Ståhl S, Uhlén M, Nygren PA. Binding proteins selected from combinatorial libraries of an alpha-helical bacterial receptor domain. Nat Biotechnol 1997;15:772–7.
17. Aunoble B, Sanches R, Didier E, Bignon YJ. Major oncogenes and tumor suppressor genes involved in epithelial ovarian cancer. Int J Oncol 2000;16:567–76.
18. Carlsson J, Nordgren H, Sjostrom J, et al. HER2 expression in breast cancer primary tumours and corresponding metastases. Original data and literature. Br J Cancer 2004;90:2344–8.
19. Gardmark T, Wester K, De la Torre M, Carlsson J, Malmstrom PU. Analysis of HER2 expression in primary urinary bladder carcinoma and corresponding metastases. BJU Int 2005;95:982–6.
20. Zidan J, Dashkovsky I, Stayerman C, Basher W, Cozacov C, Hadary A. Comparison of HER-2 overexpression in primary breast cancer and metastatic sites and its effect on biological targeting therapy of metastatic disease. Br J Cancer 2005;93:552–6.
21. Smith-Jones PM, Solit D, Afroze F, Rosen N, Larson SM. Early tumor response to Hsp90 therapy using HER2 PET: comparison with $^{18}$F-FDG PET. J Nucl Med 2006;47:793–6.
22. Whitesell L, Lindquist SL. HSP90 and the chaperoning of cancer. Nat Rev Cancer 2005;5:761–72.
23. Wikman M, Steffen AC, Gunneriusson E, et al. Selection and characterization of HER2/*neu*-binding Affibody ligands. Protein Eng Des Sel 2004;17:455–62.
24. Steffen AC, Orlova A, Wikman M, et al. Affibody-mediated tumour targeting of HER-2 expressing xenografts in mice. Eur J Nucl Med Mol Imaging 2006;33:631–8.
25. Orlova A, Magnusson M, Eriksson TL, et al. Tumor imaging using a picomolar affinity HER2 binding Affibody molecule. Cancer Res 2006;66:4339–48.
26. Tolmachev V, Nilsson F, Widström C, et al. $^{111}$In-benzyl-DTPA-$Z_{HER2:342}$, an Affibody-based conjugate for *in vivo* imaging of HER2 expression in malignant tumors. J Nucl Med 2006;74:846–53.
27. Yang D, Kuan CT, Payne J, et al. Recombinant heregulin-*Pseudomonas* exotoxin fusion proteins: interactions with the heregulin receptors and antitumor activity *in vivo*. Clin Cancer Res 1998;4:993–1004.
28. Horak EM, Heitner T, Garrison JL, et al. Engineering bispecific single-chain Fv molecules to alter signaling of the EGF receptor family. Proc Am Assoc Cancer Res 2001;42:774.
29. Steffen AC, Wikman M, Tolmachev V, et al. *In vitro* characterization of a bivalent anti-HER-2 Affibody with potential for radionuclide-based diagnostics. Cancer Biother Radiopharm 2005;20:239–48.
30. Persson M, Tolmachev V, Andersson K, Gedda L, Sandstrom M, Carlsson J. [$^{177}$Lu]pertuzumab: experimental studies on targeting of HER-2 positive tumour cells. Eur J Nucl Med Mol Imaging 2005;32:1457–62.
31. Adams GP, Shaller CC, Dadachova E, et al. A single treatment of yttrium-90-labeled CHX-A″-C6.5 diabody inhibits the growth of established human tumor xenografts in immunodeficient mice. Cancer Res 2004;64:6200–6.
32. Arora P, Oas TG, Myers JK. Fast and faster: a designed variant of the B-domain of protein A folds in 3 microsec. Protein Sci 2004;13:847–53.
33. Lub-de Hooge MN, Kosterink JG, Perik PJ, et al. Preclinical characterisation of $^{111}$In-DTPA-trastuzumab. Br J Pharmacol 2004;143:99–106.
34. Olafsen T, Tan GJ, Cheung CW, et al. Characterization of engineered anti-p185HER-2 (scFv-CH3)2 antibody fragments (minibodies) for tumor targeting. Protein Eng Des Sel 2004;17:315–23.
35. Olafsen T, Kenanova VE, Sundaresan G, et al. Optimizing radiolabeled engineered anti-p185HER2 antibody fragments for *in vivo* imaging. Cancer Res 2005;65:5907–16.
36. Robinson MK, Doss M, Shaller C, et al. Quantitative immuno-positron emission tomography imaging of HER2-positive tumor xenografts with an iodine-124 labeled anti-HER2 diabody. Cancer Res 2005;65:1471–8.
37. De Santes K, Slamon D, Anderson SK, et al. Radiolabeled antibody targeting of the HER-2/*neu* oncoprotein. Cancer Res 1992;52:1916–23.
38. Xu FJ, Yu YH, Bae DS, et al. Radioiodinated antibody targeting of the HER-2/*neu* oncoprotein. Nucl Med Biol 1997;24:451–9.

**39.** Zalutsky MR, Xu FJ, Yu Y, et al. Radioiodinated antibody targeting of the HER-2/*neu* oncoprotein: effects of labeling method on cellular processing and tissue distribution. Nucl Med Biol 1999;26:781–90.

**40.** Garmestani K, Milenic DE, Plascjak PS, Brechbiel MW. A new and convenient method for purification of $^{86}Y$ using a Sr(II) selective resin and comparison of biodistribution of $^{86}Y$ and $^{111}In$ labeled Herceptin. Nucl Med Biol 2002;29:599–606.

**41.** Behr TM, Sharkey RM, Sgouros G, et al. Overcoming the nephrotoxicity of radiometal-labeled immunoconjugates: improved cancer therapy administered to a nude mouse model in relation to the internal radiation dosimetry. Cancer 1997;80:2591–610.

**42.** Weigelt B, Peterse JL, van't Veer LJ. Breast cancer metastasis: markers and models. Nat Rev Cancer 2005;5:591–602.

**43.** Valkema R, De Jong M, Bakker WH, et al. Phase I study of peptide receptor radionuclide therapy with [In-DTPA]octreotide: the Rotterdam experience. Semin Nucl Med 2002;32:110–22.

**44.** Kwekkeboom DJ, Mueller-Brand J, Paganelli G, et al. Overview of results of peptide receptor radionuclide therapy with 3 radiolabeled somatostatin analogs. J Nucl Med 2005;46 Suppl 1:62–6S.

**45.** Rolleman EJ, Valkema R, de Jong M, Kooij PP, Krenning EP. Safe and effective inhibition of renal uptake of radiolabelled octreotide by a combination of lysine and arginine. Eur J Nucl Med Mol Imaging 2003;30:9–15.

**46.** Rolleman EJ, Krenning EP, Van Gameren A, Bernard BF, De Jong M. Uptake of [$^{111}$In-DTPA$^{0}$]octreotide in the rat kidney is inhibited by colchicine and not by fructose. J Nucl Med 2004;45:709–13.

**47.** van Eerd JE, Vegt E, Wetzels JF, et al. Gelatin-based plasma expander effectively reduces renal uptake of $^{111}In$-octreotide in mice and rats. J Nucl Med 2006;47:528–33.

**48.** Adams CW, Allison DE, Flagella K, et al. Humanization of a recombinant monoclonal antibody to produce a therapeutic HER dimerization inhibitor, pertuzumab. Cancer Immunol Immunother 2006;55:717–27.

**49.** Spector NL, Xia W, Burris Hr, et al. Study of the biologic effects of lapatinib, a reversible inhibitor of ErbB1 and ErbB2 tyrosine kinases, on tumor growth and survival pathways in patients with advanced malignancies. J Clin Oncol 2005;23:2502–12.

**50.** Baum RP, Orlova A, Tolmachev V, Feldwisch J. Receptor PET/CT and SPECT using an Affibody molecule for targeting and molecular imaging of HER2 positive cancer in animal xenografts and human breast cancer patients. J Nucl Med 2006;47:108P.